Summer 8-7-2024

A Benchtop Complex Wavefront Manipulator for Evaluating PSF Engineering

Megan Birch

A Benchtop Complex Wavefront Manipulator for Evaluating PSF Engineering

by

Megan Birch

Under the Direction of Fabien Baron and Stuart Jefferies

Thesis Submitted in Partial Fulfillment of the Requirements for the Degree of

Master of Science

in the College of Arts and Sciences

Georgia State University

2024

ABSTRACT

This research focuses on constructing a wavefront manipulation benchtop system. The primary goal is to replicate a hologram reconstruction method using a two-phase or two-pass modulation system with a spatial light modulator (SLM). The ability to precisely manipulate phase and amplitude is beneficial for simulating complex optical scenarios and enhancing astronomical observations. The chosen system allows independent control over spatial amplitude and phase distributions, improving wavefront manipulation capabilities. This precise control can be applicable across scientific, industrial, and defense sectors, enabling improved image quality and detailed analysis of low-intensity objects, a common challenge in astronomical observations and space surveillance. By constructing this benchtop setup, the research aims to create a scalable, hardware-based wavefront manipulation tool, capable of simulating various optical phenomena with high precision, offering significant potential for enhancing the observation of space objects and atmospheric conditions. The study addresses the technical challenges involved in constructing a wavefront manipulation benchtop tool for phase and amplitude modulation.

INDEX WORDS:
Wavefront Manipulation, Object Generator, Fourier Optics, Spatial Light Modulators, Light Fields, Adaptive Optics, Space Surveillance, Space Situational Awareness, Optical Simulation, Point Spread Function, Amplitude and Phase Modulation, Dual-Phase System.

ACKNOWLEDGMENTS

I would like to express my gratitude to my colleagues at the Georgia Tech Research Institute (GTRI) for their expertise, advice, and assistance in navigating the complexities of this project, including Nathan Meraz, Katie Twitchell, and Douglas Hope.

I am also grateful to Dan Johns for providing guidance and support in leveraging the Julia programming language for this research.

A special thanks to my advisors, Stuart Jefferies and Fabien Baron, for their supervision, teachings and mentorship that helped guide me through the various stages of this research.

To all those who have contributed their time, knowledge, and support, I extend my heartfelt appreciation. This work would not have been possible without your collective support.

TABLE OF CONTENTS

LIST OF FIGURES

LIST OF ABBREVIATIONS

- AO Adaptive Optics
- CCD Charge-Coupled Device
- CGH Computer-Generated Holography
- DOE Diffractive Optical Element
- F Fourier (related to Fourier Transform)
- FITS Flexible Image Transport System
- HST Hubble Space Telescope
- L-BFGS-B Limited-memory Broyden-Fletcher-Goldfarb-Shanno algorithm with Box constraints
- PSF Point Spread Function
- SLM Spatial Light Modulator
- ZOD zeroth-order diffraction

Introduction

This thesis focuses on constructing and improving a benchtop wavefront manipulation tool for applications such as Point Spread Function (PSF) engineering, inspired by the work of Jesacher et al. (2008). Their method for achieving near-perfect hologram reconstruction using spatial light modulators (SLMs) involves diffracting light through two phase holograms positioned in conjugate Fourier planes on a SLM, allowing independent control over spatial amplitude and phase distributions.

The primary goal of this research is to attempt to replicate and enhance the two-phase, two-pass modulation system proposed by Jesacher et al. (2008). The ability to precisely manipulate phase and amplitude is essential for simulating complex optical scenarios and enhancing astronomical observations. By employing this method on a benchtop setup, the research aims to advance the capabilities of wavefront propagation tools in the lab as well as simulate low-intensity objects for future applications.

"Although there are ways to encode light fields in a single phase-only diffractive optical element, it generally turns out that this requires serious trade-offs, producing for example increased speckle noise and loss of independent control over amplitude and phase of the reconstructed light field" Jesacher et al. (2008). The dual phase system was chosen to attempt to replicate due to the amplitude and phase control. In order to address SLM limitations discussed in Improso et al. (2019), while constructing the benchtop system, an additional aperture mask designed to remove unwanted high spatial frequencies, as well as

a half wave plate for polarization control of the incoming and SLM reflected beam was implemented (O'Neill (1956)). These modification aimed to provide insight in improving the quality of the object generation process for easier, clearer and more precise light field reconstructions.

1.1 Theoretical Background

Wavefront manipulation tools enable precise control over the characteristics of light fields. Among the various methods available for wavefront manipulation, the two-phase, two-pass modulation system with spatial light modulators (SLMs) was studied due to its ability to independently modulate spatial amplitude and phase distributions.

The dual-phase pass system should enhance image fidelity by allowing for the correction of phase in the Fourier domain, introduced after the Fourier transform of the initial phase discussed in Jesacher et al. (2008). This correction is achieved through precise manipulation of the light field's characteristics providing ability to independently control the amplitude and phase. This tool should provide a mechanism for addressing specific optical requirements, ensuring the integrity and accuracy of the final output image or object.

Fourier optics supports the theoretical foundation of this wavefront manipulation tool. The light fields in the Fourier conjugate planes are interconnected through Fourier transforms, which facilitate the manipulation of these fields to simulate specific optical images. The dual-pass two-phase system enables the precise shaping of these light fields, allowing for enhanced control and accuracy in simulations.

This methodology is not only effective for realistic simulations but also plays a role in the development and refinement of adaptive optics technologies (Burger et al. (2008); Roddier (1999). Adaptive optics are essential for correcting atmospheric distortions, thereby enhancing the capabilities of ground-based telescopes and other optical systems. The flexibility of the dual-phase approach can benefit a wide range of optical scenarios, supporting advancements in both research and practical applications.

1.2 Mathematical Framework

The underlying principles of this object generation module are grounded in Fourier optics, which facilitates the manipulation of light fields to simulate specific optical images by converting a spatial light distribution into its frequency components. The mathematical framework for using spatial light modulators to reconstruct images through the manipulation of wave fields employs these Fourier optic principles to modulate the amplitude and phase of light fields, enabling the simulation and reconstruction of complex objects such as images of the Hubble Space Telescope (HST).

1.2.1 Complex Wave Fields and Fourier Optics

A light field in the object plane can be expressed as a complex wave field:

$$A(x, y) = |A(x, y)|e^{j\Theta(x,y)} \tag{1.1}$$

where $A(x, y)$ represents the light field in the object or spatial domain, $|A(x, y)|$ signifies

the absolute amplitude in the spatial domain, and $\Theta(x, y)$ denotes the phase for that light field. (Abbott et al. (2022)) Here, x and y are spatial coordinates and j is the imaginary unit. The transformation of the light field in the spatial domain to the frequency domain is created from the Fourier Transform (Miura (2003)). The complex light field in the frequency domain or Fourier plane is expressed as:

$$a(u, v) = \mathcal{F}\left[|A(x, y)|e^{j\Theta(x,y)}\right] \tag{1.2}$$

where $|a(u, v)|$ is the complex modulus of the light field in the frequency domain and u and v are the frequency variables corresponding to x and y. $\theta(u, v)$ denotes the phase in the frequency domain. Here a(u,v) is the plane wave spectrum of $A(x, y)$. The corresponding Fourier transform pairs are then:

$$A(x, y) = \mathcal{F}\left[|a(u, v)|e^{-j\theta(u,v)}\right] \tag{1.3}$$

1.2.2 Fourier Optics

To convert the light field from the spatial domain to the frequency domain, a Fourier transform is applied. For a wave field A(x,y) in the frequency domain, its Fourier transform is given by Jeffries (2024); Suchkov et al. (2019):

$$A(u, v) = \mathcal{F}\{A(x, y)\} = \int_{-\infty}^{\infty}\int_{-\infty}^{\infty} A(x, y)e^{-j2\pi(ux+vy)}dxdy \tag{1.4}$$

Where $\mathcal{F}$ represents the Fourier Transform function. Conversely, the inverse Fourier transform, which reconstructs the spatial domain optical field from its frequency components,

is defined as:

$$A(x,y) = \mathcal{F}\{A(u,v)\} = \int_{-\infty}^{\infty}\int_{-\infty}^{\infty} A(u,v)e^{j2\pi(ux+vy)}dudv \tag{1.5}$$

To create a specific light field, such as a laser beam, using Equation 1.1 in the object plane, requires the definite complex field defined in Equation 1.2 in the Fourier plane. This can be expressed as Jesacher et al. (2008):

$$A(u,v) = \frac{1}{\lambda f}\int_x\int_y A(x,y)\exp\left(-i\frac{2\pi}{\lambda f}(ux+yv)\right)dxdy \tag{1.6}$$

Here, λ is the laser wavelength and f is the focal length of the Fourier-transforming lens. $|A(u,v)|$ is now defined as the laser beam amplitude for a specific light field.

1.2.3 Phase Modulation and Image Reconstruction Utilizing Two Phases

To modulate the optical field for an object generator, we use the equations 1.2 and 1.3 where the $|\alpha(u,v)|$ is the object modulus in the frequency domain and $\theta(u,v)$ is the phase corresponding to the generated object. The below equations defined for the image reconstruction of the benchtop setup:

$$a_L(u,v) = \mathcal{F}\left[|A_L(x,y)|e^{j\Theta_L(x,y)}\right] \tag{1.7}$$

$$A_O(x,y) = \mathcal{F}\left[|a_O(u,v)|e^{-j\theta_O(u,v)}\right] \tag{1.8}$$

Where A_O and a_0 represent the object light field from the image that is being reconstructed and A_L and a_L represent the laser light field.

Below represent the definitions for each set of wave fields and the generated phases in order to reconstruct the image.

$$\psi = \mathcal{F}[|A_L(x,y)|e^{j\theta}] \tag{1.9}$$

where ψ represents the first phase applied to the SLM.

$$\beta = \mathcal{F}\left\{A_O(x,y)e^{j(\theta-\phi)}\right\} \tag{1.10}$$

Where β is the second phase applied to the SLM and ψ is the phase created from the Fourier transform of the superimposed laser amplitude and first phase.

$$o(u,v) = \mathcal{F}[\mathcal{F}[A_L(x,y)^{j\psi(x,y)}] \cdot A_O(x,y)e^{j\beta(x,y)}] \tag{1.11}$$

$o(u,v)$ represents the final image reconstructed. Given these equations we can generate a phase from the laser amplitude that, when Fourier transformed, will produce the amplitude of the generated object. A second phase will be generated to superimpose with the new amplitude followed by a Fourier transform that will produce the generated object of interest.

$a_O(x,y)$ can be directly shaped by the element θ_O in the Fourier plane on the SLM phase screen, but not its amplitude. Thus the modulus of the object field, $a_O(u,v)$, must be created by Fourier transforming a generated phase, ψ located in plane 1 as the first phase

mask on the SLM. Using the laser amplitude in the spatial domain, $|A_L(x, y)|$, the phase ψ is generated so that when superimposed with the laser amplitude, $|A_L(x, y)|$, produces the generated or simulated object $a_O(x, y)$. Performing the Fourier transform then produces the needed modulus in the frequency domain, $|a_O(u, v)|$ of the object field.

ψ can be iteratively optimized using specific phase DOE design algorithms such that it creates the desired modulus $|a_O(u, v)|$ in the Fourier plane when it is homogeneously illuminated. However, a consequence of this optimization procedure is that the field created by ψ in the second pupil plane, designated by β will have a randomly distributed phase ϕ. Although the phase ϕ cannot be controlled directly, it is known and the second phase mask can be generated to eliminate this unwanted phase once superimposed.

The idea is to modify ϕ by β such that the result is θ_O. Consequently, the second phase, β has to be calculated by: $\beta = \theta - \phi$ Because SLMs are restricted to 0-255, the phases must be generated with an interval from 0-2π. Altogether, this procedure generates the desired complex field $o(u, v)$ directly behind the second phase mask β, and hence also $A(x, y)$ in the object plane. Theoretically, no light is lost since the method solely utilizes non-absorbing phase elements (Jesacher et al. (2008)).

The final image is obtained by placing the calculated phases ψ, β, and incorporating ϕ as needed, on the SLMs and taking the Fourier transform of the complex optical field. The mathamatical framework to calculate ψ and β is shown below:

1.2.4 Solving for the Two Phases

Solving for the two phase screens β and ψ required for an SLM to generate an object, we start with the object field $o(x, y)$ and apply the Inverse Fourier Transform to Both Sides of the equation:

$$\mathcal{F}\{a(x,y)\} = \mathcal{F}\left\{A(x,y)e^{j\psi(x,y)}\right\} \cdot \beta(x,y) \tag{1.12}$$

Now solving for $\beta(u, v)$:

$$\beta(u,v) = \frac{o(u,v)}{\beta(u,v)} \tag{1.13}$$

Thus, $\beta(x, y)$ can be written as:

$$\beta(x,y) = \frac{\mathcal{F}\{o(x,y)\}}{\mathcal{F}\left\{A(x,y)e^{j\psi(x,y)}\right\}} \tag{1.14}$$

Now isolating $\psi(x, y)$ from equation 1.9:

$$\psi(x,y) = \frac{\ln(a(x,y)) - \ln(A(x,y))}{j} \tag{1.15}$$

Since $\frac{1}{j} = -j$:

$$\psi(x,y) = -j[\ln(a(x,y)) - \ln(A(x,y))] \tag{1.16}$$

This mathematical framework not only explains the process of image reconstruction and optimization but also emphasizes the critical role of Fourier transforms in bridging the fre-

quency and spatial domains, pivotal for applications like spatial light modulators, which necessitate precise amplitude and phase adjustments for optimal image projection.

Experimental Setup

The experimental setup for the object generation module, which employs the two-phase pass system, is meticulously designed to ensure precise control and manipulation of light properties. This setup is essential for simulating complex optical phenomena, particularly when addressing the challenge of imaging two closely spaced objects of significantly different luminosities, such as an exoplanet orbiting a star. In such scenarios, the Point Spread Function (PSF) of the fainter object is often obscured by the brighter object's intensity (Hope (2019)).

The experimental setup revolves around three main components: the spatial light modulator (SLM), a series of lenses, and an aperture, all orchestrated to modulate and analyze light in a controlled environment. The system begins with a coherent visible light source, providing a stable and controllable beam of light. This light is first collimated using single-mode fibers and achromatic lenses to ensure it maintains uniformity and direction over distances.

The first critical component in the setup is the spatial light modulator (SLM), which is configured to introduce an initial phase perturbation to the light beam. This phase perturbation is calculated to modify the beam's wavefront, setting the stage for the generation of the target. The modulated light then passes through the first lens, which performs a Fourier transform on the beam. This transform shifts the light from the spatial domain to the frequency domain, creating a distribution that represents the phase-modulated light pattern or an image representing the Fourier amplitude distribution of the desired object (Tyson

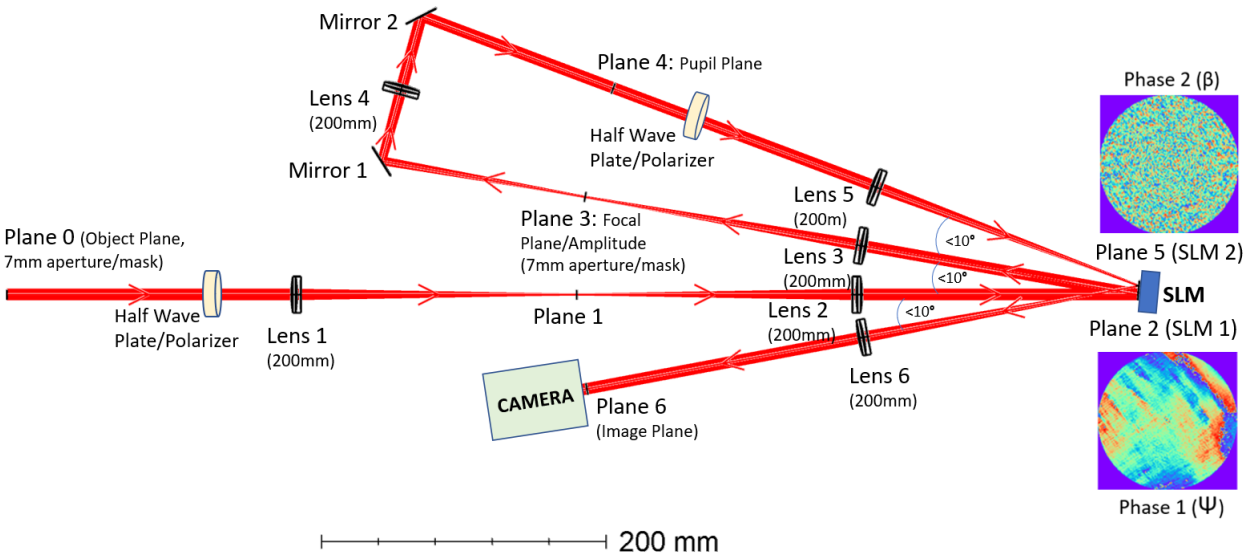

Figure 2.1 *Schematic of the experimental optical wavefront manipulator benchtop setup. An achromatic lens is used to collimate the light emanating from a linearly polarized 637 nm laser through a 5-micron single mode fiber before the shown benchtop setup. The object generator benchtop begins with a focal plane mask to create a 7mm aperture. Following this, a half-wave plate adjusts the polarization originating from the single mode fiber to reduce the intensity of the zeroth-order diffraction (ZOD) spots caused by subsequent spatial light modulators (SLMs). A set of lenses are then used to relay the beam aperture onto the SLM. The first phase is placed on the first pass of the SLM in the pupil plane, followed by a 4F system and a second aperture mask. The 4F system preforms a Fourier transform to produce the amplitude of the original image followed by a relay system to relay this amplitude onto the second half of the SLM. The second phase is placed on SLM in the focal plane, in order to superimpose the amplitude and simulated phase. This is then followed by a 2F system to place the image on the camera sensor. The displayed images next to the SLM show the two phase screens added to the SLM. Each angle associated with the SLM was less than 10 degrees to maintain optimal performance, efficiency, and accuracy of the optical system.*

(2014)).

After the Fourier transform, the beam encounters an aperture mask strategically placed at the focal plane. The width of the mask is matched to the beam's width on the SLM. This step helps maintain the integrity of the modulation and focuses the system on the necessary frequency components by filtering out higher spatial frequencies beyond the desired

spectrum, refining the amplitude information in the beam. (Blinder et al. (2022))

The beam, now carrying the tailored amplitude information and an extraneous phase, is directed through a second lens. This lens restores the beam to a collimated state, ensuring that it remains parallel and focused for the subsequent phase modulation process. This lens also acts as a relay system with the third lens guiding the focused beam back onto the SLM for a second phase modulation.

This second modulation is designed to refine the phase adjustments based on the outcomes of the first modulation and to incorporate the necessary corrections that align with the simulation's objectives. It compensates for any spurious phases introduced during the initial modulation and aligns the final phase properties with the target's characteristics.

The light beam, now encoded with both the correct amplitude and phase information, passes through a final lens that performs another Fourier transform. This transform converts the frequency components back into a spatial light distribution, which is the final image of the target object. This image is then captured and analyzed using a camera, allowing researchers to study the simulated effects and validate the system's performance.

This elaborate setup requires micro meter level precision or alignment and through its sequential manipulation of the light beam's phase and amplitude, enables the creation of detailed optical simulations (Jesacher et al. (2008); Arines & García (2020)). By carefully controlling these properties and employing Fourier optics principles, the system can simulate a wide variety of optical targets with high fidelity. The inclusion of aperture masks and the strategic use of SLM for dual-phase modulation are critical for achieving the desired

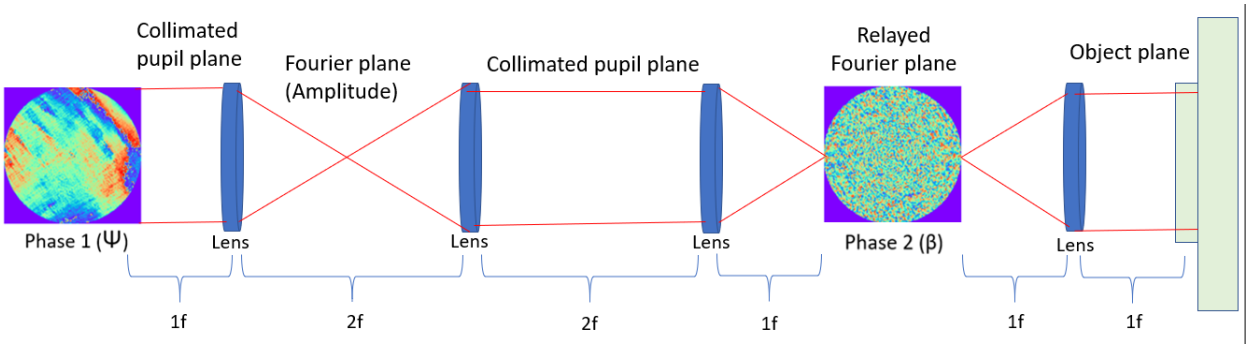

Figure 2.2 *Starting with phase 1, converting to the Fourier domain for amplitude construction, relaying the focal plain back onto the SLM, followed by a Fourier transform to image in the object plane.*

outcome of simulating objects with precise amplitude and phase characteristics. (Blinder et al. (2022)) This process highlights the power of Fourier optics in advanced imaging and simulation applications, offering a versatile tool for research, education, and technological development in the field of optics.

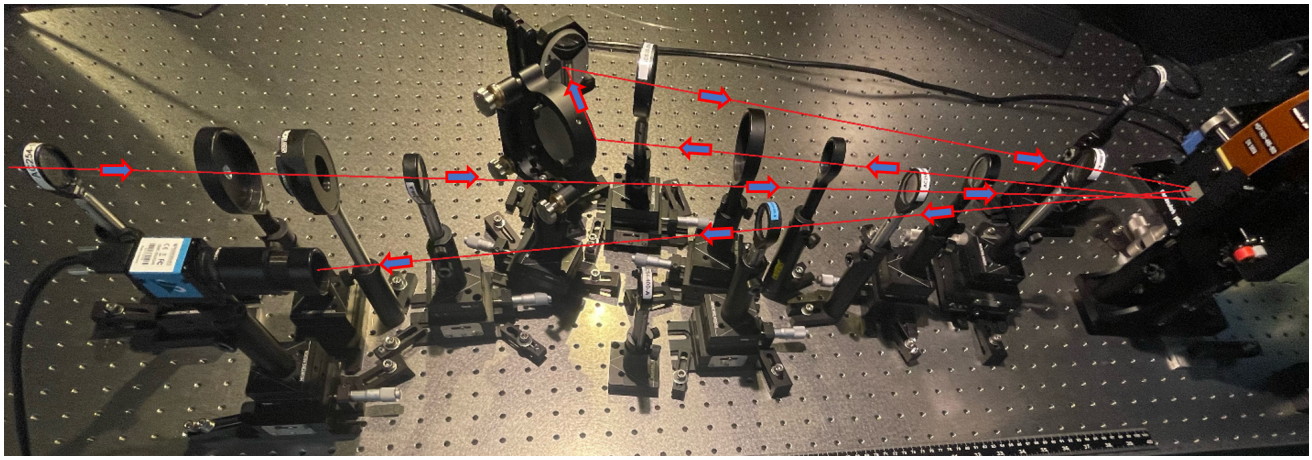

Figure 2.3 *The red line represents the beam path. All optics are on kinematic mounts and x stages for fine tune alignment adjustments. Note lens path lengths were adjusted post image.*

2.1 Simulation and Modeling Tools

This section details the functionality of the model used in this thesis, originally developed by Dr. Jefferies and Dr. Baron. Their contributions have been instrumental in the successful implementation and adaptation of these methods for the specific research objectives.

Initially, the model loads and normalizes a target image from a FITS file. The wavefront data is then manipulated by applying phase corrections and adjustments. To generate the phases, the code first computes the Fourier transform of the wavefront data. This transformation shifts the data from the spatial domain (x, y) to the frequency domain $(u, v$, making it easier to analyze and manipulate. In the frequency domain, the phase information is extracted from the complex wavefront data. The phase of each point in the wavefront is crucial for accurately reconstructing the image, as it contains information about the light's path and interference patterns.

2.1.1 Aperture

A circular aperture mask is generated to define the system's spatial frequency cutoff, adhering to the Nyquist sampling criterion. The Nyquist criterion ensures that the sampling rate is sufficient to capture the necessary detail in the image without aliasing. Mathematically, the Nyquist frequency is given by:

$$f_N = \frac{1}{2\Delta x} \tag{2.1}$$

where Δx is the sampling interval. (Jeffries (2024))

The phase retrieval process involves the definition of two complex pupil functions, one representing the base phase defined in Equation 1.11 and the other scaled by a predetermined amplitude profile defined in Equation 1.13.

2.1.2 Amplitude

To create a Gaussian amplitude profile to represent the lab laser amplitude, the code defines a grid of x and y coordinates ranging from -1 to 1, matching the dimensions of the image. A Gaussian function is then applied to this grid to create the profile. The Gaussian amplitude profile $G(x, y)$ is given by:

$$G(x, y) = \exp\left(-\frac{x^2 + y^2}{2\sigma^2}\right) \tag{2.2}$$

where σ is the standard deviation of the Gaussian profile, controlling the spread of the Gaussian function. In this code, σ is set to 0.3. The code uses the `numpy` library to create the grid and compute the Gaussian profile.

2.1.3 Error Metric Calculation

The optimization of pixel values, aiming to accurately represent the object $o(u, v)$, is achieved by minimizing the error metric ϵ, a sum of squared differences between the actual pixel values o_n and the calculated values $a_n a_n^*$, as detailed in the equation:

$$\epsilon = \sum_n (o_n - a_n a_n^*)^2 \tag{2.3}$$

where: o_n is the actual pixel value of the object, a_n is the calculated pixel value, and a_n^*

is the complex conjugate of a_n. (Abbott et al. (2022))

To refine this optimization, especially in contexts utilizing gradient information for minimization, it is essential to compute the partial derivatives of ϵ with respect to both the real and imaginary components of A_m, leading to equations that use $\frac{\partial \epsilon}{\partial A_{r_m}}$ and $\frac{\partial \epsilon}{\partial A_{i_m}}$, respectively. A_M) refers to the complex amplitude in the frequency domain at a specific spatial frequency index m. These derivatives are foundational for adjusting A_m to minimize ϵ, enhancing the accuracy of the image representation. (Jeffries (2024))

2.1.4 Optimization and Gradient Calculation

To optimize the phases ψ and β that generate the desired image, we use gradient-based methods. The gradients of the error metric with respect to the phases are calculated as follows: (Jeffries (2024))

The gradient with respect to ψ is:

$$\frac{\partial \epsilon}{\partial \psi} = 4\Im\left[\delta\right] \tag{2.4}$$

The gradient with respect to β is:

$$\frac{\partial \epsilon}{\partial \beta} = 4\Im\left[\zeta\right] \tag{2.5}$$

Where:

$$\delta = \mathcal{F}\left[pupil_p \cdot \mathcal{F}[\eta \cdot \mathcal{F}[pupil_b]]\right] \tag{2.6}$$

$$\zeta = \mathcal{F}\left[\alpha \mathcal{F}[pupil_b \cdot \eta]\right] \tag{2.7}$$

$$\eta = \mathcal{F}\left[\overline{a}\mathcal{F}[\text{resid}]\right] \tag{2.8}$$

Here, $\psi(u, v)$ and $\beta(u, v)$ are the phases applied to SLM#2 and SLM#1. $pupil_p$ is the pupil function for SLM#2, $pupil_b$ is the pupil function for SLM#1. $\Im$ denotes the imaginary part of the complex number. resid(x, y) represents the residual error between the observed data and the model. $\eta(x, y)$ is an intermediate variable used in the calculation of the gradient.

By iteratively optimizing the phases ψ, β, and incorporating ϕ as needed, we minimize the error metric ϵ and reconstruct an image that closely matches the object image $o(u, v)$.

These pupil functions are updated iteratively through the optimization of a cost function, which quantifies the squared error between the observed data and the model generated by Fourier transforming the modulated pupil functions. The cost function C is defined as:

$$C = \sum_{u,v} \left| o(u, v) - a(u, v)a^*(u, v) \right|^2 \tag{2.9}$$

where: $o(u, v)$ represents the observed data, $a(u, v)$ is the reconstructed image, and $a^*(u, v)$ is the complex conjugate of $a(u, v)$. The Fourier transform used to reconstruct the spatial domain light field from its frequency components is defined in section 1.2.2.

The optimization employs the L-BFGS-B algorithm, a limited-memory variant of the Broyden–Fletcher–Goldfarb–Shanno algorithm, suitable for problems with large numbers of variables. The gradient of the cost function with respect to the phase components ψ and β is used to update the pupil functions iteratively. The gradient with respect to ψ is:

$$\frac{\partial C}{\partial \psi} = 4\Im\left[\mathcal{F}\left\{P_2(x,y)\cdot\mathcal{F}\left[\eta(x,y)\cdot\mathcal{F}\left\{P_1(x,y)\right\}\right]\right\}\right] \tag{2.10}$$

where again, $\mathcal{F}$ denotes the Fourier transform, $P_1(x,y) = A(u,v)e^{j\psi(u,v)}$ is the first complex pupil function. $|(A(u,v)|$ represents the amplitude profile in the frequency domain. $\psi(u,v)$ represents the phase component of the first pupil function. $P_2(x,y) = A(u,v)e^{j\beta(u,v)}$ is the second complex pupil function. $\beta(u,v)$ represents the phase component of the second pupil function. $\beta(x,y) = a(x,y)\cdot\mathcal{F}\{\text{resid}(x,y)\}$ is an intermediate variable used in the calculation of the gradient. Here, $a(x,y)$ is the reconstructed image in the spatial domain. resid(x,y) represents the residual error between the observed data and the model, defined as resid$(x,y) = o(x,y) - a(x,y)$, where $a(x,y)$ represents the modeled data. $\Im\{\cdot\}$ denotes the imaginary part of a complex number and o(x, y) represents the optical bench generated object. Lastly, C represents the cost function, which quantifies the squared error between the observed data and the model generated by Fourier transforming the modulated pupil functions.

The optimization process iteratively updates the phase components ψ and β to minimize the cost function C. This minimization process aims to reduce the discrepancy between the observed data and the reconstructed image, leading to a more accurate image reconstruction.

Combining terms and writing the observed data or final object image in one equation produces:

$$o(u,v) = \mathcal{F}[\mathcal{F}[G(x,y)^{j\psi(x,y)}]\cdot A_O(x,y)e^{j\beta(x,y)}] \tag{2.11}$$

where: $G(x, y) = \exp\left(-\frac{x^2+y^2}{2\sigma^2}\right)$ is the Gaussian amplitude profile and $A_O(x, y)e^{j\beta(x,y)}$ are the complex pupil functions.

This equation describes the entire process from the initial Gaussian amplitude $G(x, y)$ through the modulation by the pupil functions $\psi(x, y)$ and $\beta(x, y)$, as well as the transformation via Fourier and inverse Fourier transforms to obtain the final reconstructed image $o(u, v)$.

The final reconstructed phases and the corresponding image are visualized alongside the original data. The optimization continues until the cost function converges to a minimum, providing the optimal phase retrieval for the reconstructed image. The two phases are then scaled and meticulously placed on a bitmap image file (BMP) within pixel accuracy, representing the phase screen of the SLM. This method provides a robust framework for astronomical image reconstruction, facilitating deeper insights into the underlying physical processes.

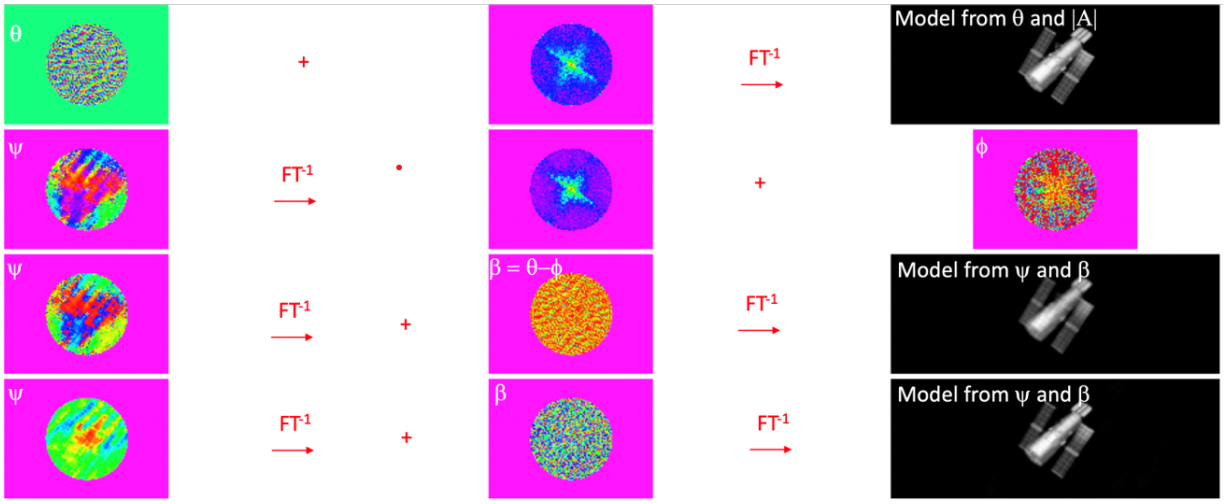

Figure 2.4 *Row 1 represents the phase θ and amplitude that when transformed and taking the absolute value, produces the original image. In the second row, the model then solves for phase ψ that when transformed gives amplitude from the original image and extra phase ϕ. The third row provides the images produced if the two phases were placed on the SLM. The last row shows the two phases the model creates after many iterations to try and replicate the previous image, that will actually be placed on the SLM.*

Data and Analysis

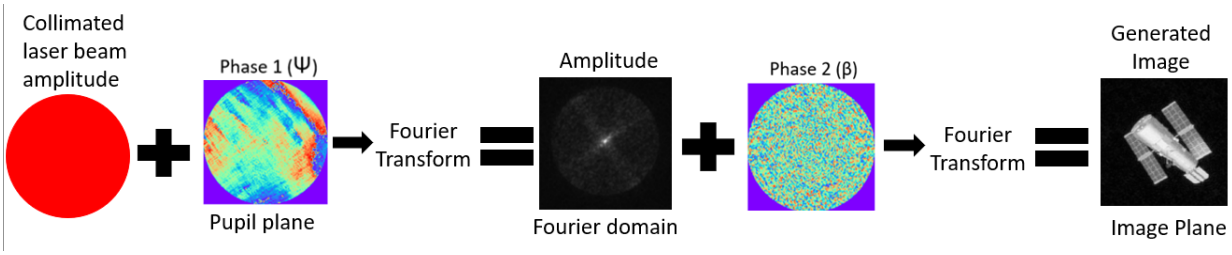

Figure 3.1 *The initial laser amplitude is superimposed with the generated phase one on the SLM. The Fourier transform of the combined amplitude and phase produce the amplitude of the generated image. The inverse Fourier transform of this amplitude superimposed with the second generated phase produce the final generated image.*

Figure 3.1 provides a visual representation of how the mathematical model is translated into the physical setup on the benchtop. The diagram illustrates the process starting with the initial laser amplitude, which is then superimposed with the first generated phase on the Spatial Light Modulator (SLM). This combined amplitude and phase undergo a Fourier transform, resulting in the amplitude of the generated image.

Next, the inverse Fourier transform of this amplitude, combined with the second generated phase, produces the final generated image. This process visually encapsulates the steps described in the mathematical model, particularly the application of the Fourier and inverse Fourier transforms as outlined in Equation 2.3. The figure effectively bridges the theoretical concepts with their practical implementation, demonstrating how precise control over phase and amplitude manipulation on the benchtop mirrors the mathematical framework.

3.1 Model Simulation Results

The design and alignment of the optical system was first modeled using Zemax, an optical design software that enables detailed simulation and analysis of optical systems. Zemax allowed for the simulation of the light path in both the frequency and spatial domains, providing a comprehensive understanding of how the system would function before physical construction. This modeling helped ensuring the theoretical design could be translated into a practical setup.

Zemax simulations helped visualize the propagation of light through the optical system, from the source to the final image on the detector. By simulating the system, potential issues with alignment, phase modulation, and light propagation could be identified and addressed.

Figure 3.2 illustrates the output of the simulation model for the two phases to be added onto the SLM. The figure shows the original image of Hubble, the modeled image expected on the benchtop, the amplitude to be created on the benchtop, and the two phases to be placed on the SLM.

The top row of Figure 3.2 shows, from left to right, the original Hubble image used to generate the phases, the expected output image after passing through the dual-phase setup, and the output image rendered in 8-bit form to accommodate the limitations of the SLM. The bottom row illustrates the amplitude image with the masked aperture, which can be compared to the amplitude on the benchtop after the first SLM pass, the phase applied during the first SLM pass, and the phase applied during the second SLM pass.

Through the Zemax model, it became apparent that the initial setup did not allow the

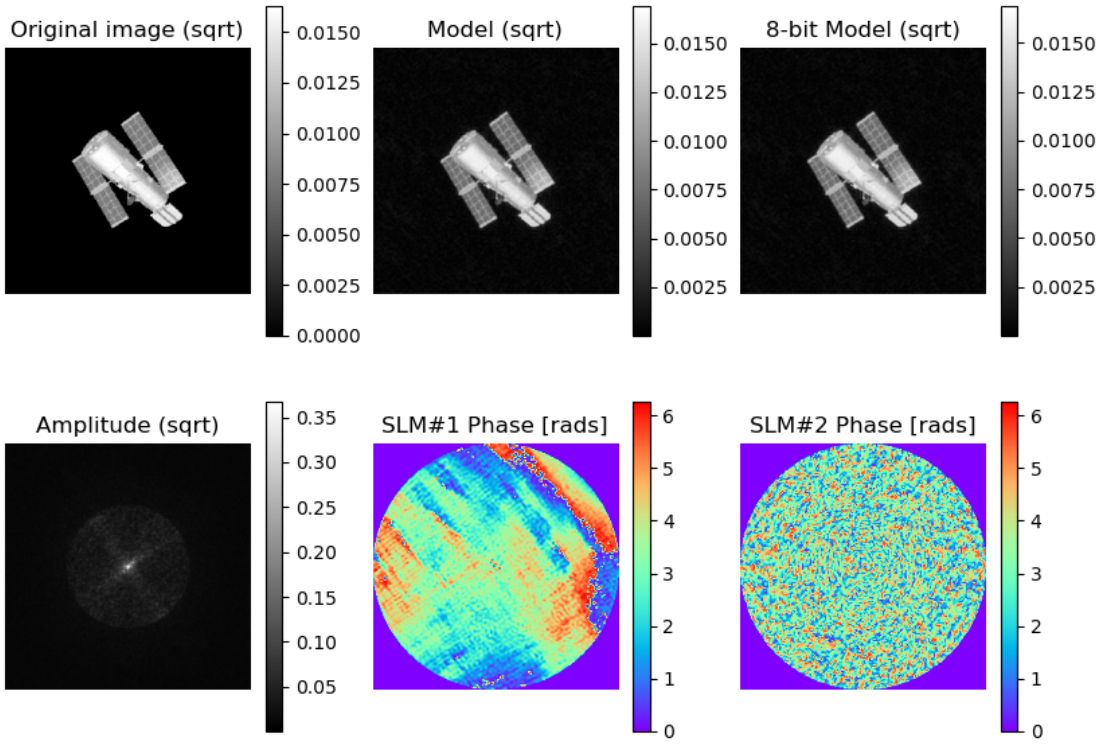

Figure 3.2 *Top row: From left to right, the original image used to reproduce the phases, the output image after the dual-phase benchtop, and the output image after the dual-phase benchtop in 8-bit form due to the SLM limitations. Bottom row: From left to right, the amplitude image with the masked aperture, which can be compared to the amplitude in the benchtop after the first SLM pass, the phase placed on the first SLM pass, and the second phase placed on the second SLM pass.*

two planes to superimpose correctly, leading to no image reconstruction. To address this issue, I had to swap lenses, adjust the lengths between optical components, and re-align the system. These adjustments were guided by the insights gained from the Zemax simulation, which highlighted the specific modifications needed to correct the setup. After making these

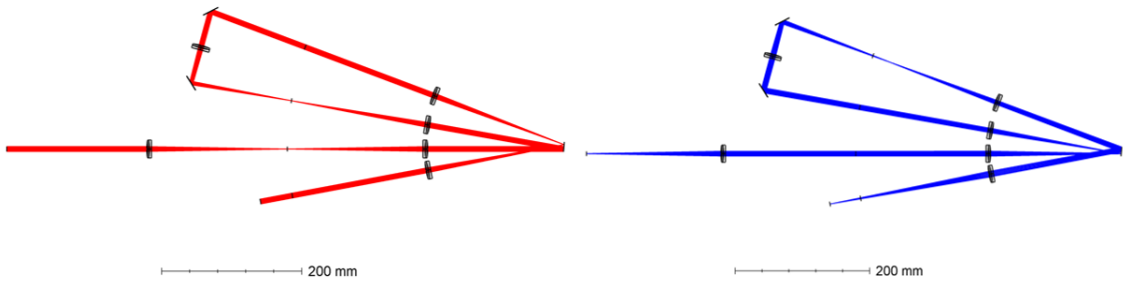

Figure 3.3 *These models were used to understand and optimize the light path and phase modulation during physical implementation.*

changes, I was able to focus both the phase and amplitude on the same plane.

Using Zemax bridged the gap between a theoretical design and practical implementation. The simulation helped identify and address potential issues, optimize the alignment and configuration of the optical components, and ensure that the system would function as intended. This modeling step significantly reduced the discovered errors and contributed to the overall success of the project.

3.2 Alignment

Achieving perfect alignment in an optical system is a significant challenge, particularly when dealing with two phases. While alignment is more straightforward with a single phase, introducing a second phase increases complexity exponentially. The goal was to make two phases overlap perfectly, which required precise adjustments and meticulous troubleshooting.

One major difficulty was achieving 1-pixel alignment when the point spread function of the laser was 20 micrometers. This required not only careful manual adjustments but also the use of mathematical techniques to ensure precision. The alignment techniques employed included precise lens alignment, careful SLM alignment, determining the correct phase size

and pupil size, and ensuring that the pupil location on the SLM was within 1-pixel alignment. Additionally, confirming that both the focal plane and pupil plane were in focus was essential for achieving an aligned set up.

To achieve precise lens alignment, high-precision mounts were used, and careful adjustments ensured that lenses were perfectly positioned along the optical axis. Kinematic magnetic mounts allowed for the easy removal and re-alignment of lenses without disturbing the beam path. For the SLMs, meticulous positioning was required to ensure that the phase patterns were correctly aligned with the optical axis. This process necessitated iterative adjustments and verification to minimize alignment errors.

Throughout this process, iterative adjustments and testing were necessary to debug and refine the alignment. Small, precise changes were made, and their effects on the system's performance were observed to achieve the best possible alignment. This iterative approach was essential for overcoming the challenges posed by the dual-phase system.

Various resources and experts, including an optics Ph.D. student, an astronomy Ph.D. student, an optics engineer, and optics professors, were consulted to address the challenges encountered. Their insights and guidance were invaluable in resolving persistent issues. Despite the resources available in the lab, some limitations persisted, preventing the attainment of optimal reconstructed results.

The alignment process in a dual-phase optical system is intricate and requires a high degree of precision. The techniques employed, combined with iterative adjustments and expert consultations, were crucial in achieving the best possible alignment given the con-

straints. Future improvements, such as automation and higher-resolution components such as motorized mounts, may further enhance the alignment accuracy and system performance.

3.3 Amplitude

The amplitude of the laser in the pupil plane was a critical factor in the model, as it directly influenced the accuracy and quality of the generated phase images. Initially, an image of the laser's amplitude was captured and used as the starting amplitude for the model. However, this initial amplitude image presented several challenges. It was notably flat, and the scaling was off compared to the produced phases, leading to resolution issues in the final images. Additionally, dust on the camera sensor caused incorrect phase production, further complicating the process.

Due to these significant issues with the initial laser amplitude image, it was determined that an alternative approach was necessary. A Gaussian amplitude profile was employed to represent the initial amplitude more accurately. This profile was chosen because it better approximates the expected intensity distribution of a laser beam in the pupil plane, providing a smoother and more consistent starting point for phase generation.

The flatness and inherent noise in the captured amplitude image had previously impacted the quality of the final output. By switching to a Gaussian model, the amplitude profile became more representative of the ideal beam characteristics. This change was crucial in reducing the discrepancies that had arisen from the original flat amplitude image, which had led to poor resolution and detail in the phase images.

The presence of dust on the camera sensor had also most likely introduced localized distortions in the amplitude image, further degrading the phase calculations. These distortions resulted in unwanted phase variations and artifacts in the final images. By adopting a Gaussian model, these issues were mitigated, as the synthetic profile was free from physical contaminants and noise.

3.4 SLM Flat Phase Screens

The laser beam in the optical setup interacts with two Spatial Light Modulators (SLMs) on the optical bench before entering the wavefront manipulation benchtop. Each SLM can introduce wavefront errors and aberrations due to inherent distortions in the system. To correct these issues and improve image quality, a flat phase screen must be added to each SLM. This subsection discusses the necessity of applying a flat phase image to the SLMs and the impact on the wavefront.

SLMs can introduce wavefront distortions that degrade the quality of the optical system's output. These distortions arise from imperfections in the SLM surface and inconsistencies in the modulation process. To mitigate these effects, a uniform phase correction, or flat phase, is applied across the entire SLM surface. This flat phase serves to counteract any inherent distortions, ensuring that the wavefront errors are minimized.

Figure 3.4 provides an example of a flat phase implemented onto the SLM phase screen.

By applying this flat phase, the SLM can correct for wavefront errors and minimize aberrations, resulting in a more accurate and clearer diffraction pattern. This correction

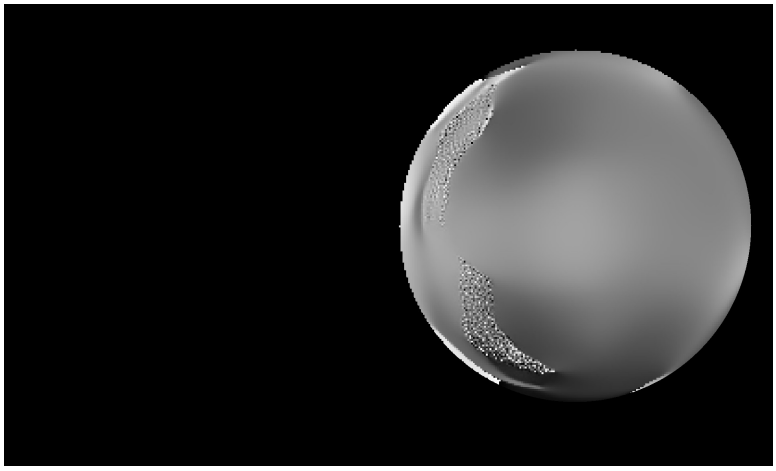

Figure 3.4 *Left: A flat image implemented onto the SLM phase screen for correction purposes.*

is crucial for optimizing the optical performance and enhancing the fidelity of the final images produced by the system. The application of a flat phase ensures that the wavefront entering the wavefront manipulation benchtop is as close to ideal as possible, providing a solid foundation for subsequent manipulations.

The need to add a flat image to the SLMs where the beam is located is critical for achieving precise control over the wavefront. Without this correction, the inherent distortions in the SLMs would propagate through the system, compromising the accuracy and clarity of the final output. By implementing flat phase screens, the optical system can maintain a high degree of fidelity, essential for applications requiring precise wavefront manipulation and image quality, such as PSF engineering and astronomical observations.

3.5 Zeroth-Order Diffraction

In optical systems utilizing Spatial Light Modulators (SLMs), ZOD can significantly impact the quality of imaging by introducing an unwanted bright spot at the center of the diffraction

pattern. To mitigate this effect, a blazed grating can be applied to the SLM. A blazed grating is designed to redirect most of the diffracted light into a specific diffraction order by optimizing the grating profile, thus minimizing the intensity of the zeroth-order beam.

To illustrate the benefits of this technique, consider two images in figure 3.5 produced by the SLM: one without a blaze grating and one with a blaze grating applied. The first image, obtained without a blaze grating, shows a prominent zeroth-order spot at the center of the diffraction pattern, which obscures the desired diffraction features and reduces overall image contrast. This unwanted ZOD n not only interferes with the visual clarity of the target pattern but also compromises the accuracy of any measurements or analyses based on the image.

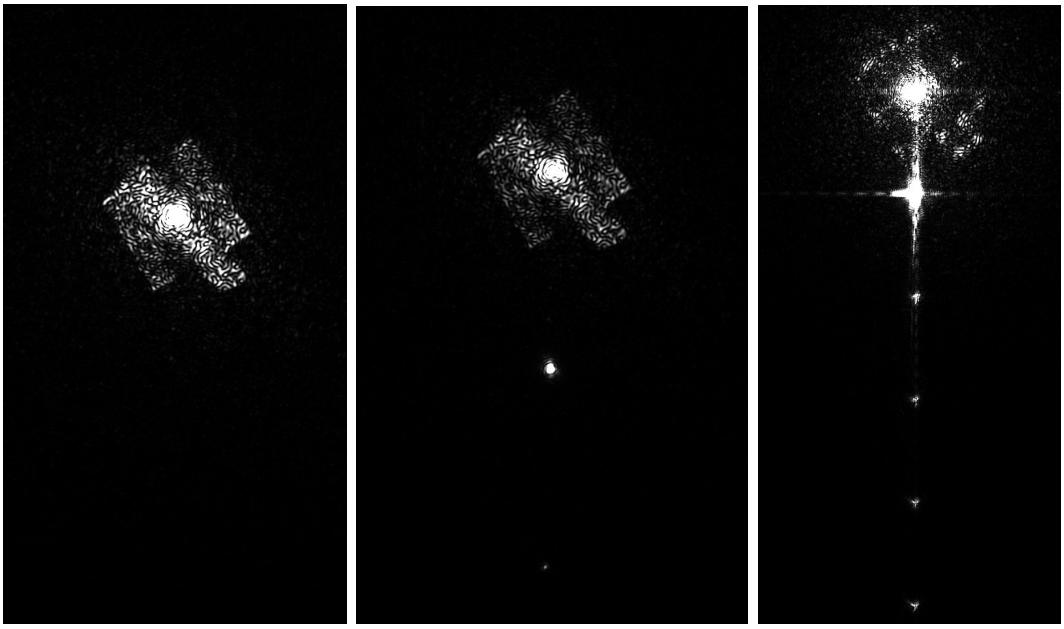

Figure 3.5 *Left: Effects of the SLM's ZOD impacting the center of the image. Middle: Blaze grating applied to minimize the diffracted light effects on the final image. Right: Blaze grating applied to the second SLM to minimize final image diffracted light effects.*

In contrast, the second image, produced with a blaze grating applied to the SLM, demon-

strates an improvement where the center beam is minimized. The blaze grating effectively redirects the zeroth-order beam away from the optical axis, thereby reducing its intensity and minimizing its impact on the image. This results in a cleaner diffraction pattern with enhanced contrast and better separation of the desired diffraction orders. The blaze grating's design ensures that the majority of the incident light is diffracted into the intended orders, providing a more accurate representation of the optical system's performance.

The comparison of these two images demonstrates the significant advantage of using a blaze grating in SLM applications. By applying this technique, the quality of the optical imaging is notably enhanced, leading to clearer and more precise diffraction patterns, which is crucial for applications such as holography, beam shaping, and optical trapping.

In addition to applying a blaze grating, masking was implemented in the light path to further enhance the quality of the diffraction patterns by selectively blocking unwanted diffracted light. A spatial filter was strategically placed in the frequency Fourier plane of the optical system to intercept and block the zeroth-order beam as well as other unwanted diffraction orders. This mask was carefully designed to match the spatial frequency components of the diffracted light, ensuring that only the desired diffraction orders passed through while the undesired components were attenuated.

The implementation of this masking involved precise alignment of the spatial filter with the optical axis and the diffracted light pattern. By blocking the zeroth-order beam, the mask significantly reduced the interference and noise caused by undiffracted light. Furthermore, by filtering out higher-order diffraction components that did not contribute to the desired image,

the mask improved the overall contrast and clarity of the resulting diffraction pattern. This combined approach of using a blaze grating and spatial masking provided a robust solution to enhance image quality in SLM-based optical systems, ensuring that the final images were free from extraneous light and accurately represented the intended optical phenomena.

The right image in 3.5 vividly illustrates the challenges posed by using only the phase of the Hubble Space Telescope through the entire system. The resulting image is marred by significant errors and aberrations, highlighting the inherent imperfections within the optical setup. These defects and a lack of clarity, underscoring the system's inability to faithfully reproduce the intended image. This serves as a stark indicator of the obstacles faced when attempting to achieve a precise final image. The compounded errors from the system make it highly unlikely to accurately visualize the final image when combining two phases, demonstrating the critical need for further refinement and optimization of the optical configuration.

3.6 Masking

The use of aperture masks was a critical component in refining the quality of the images generated by the optical system. Higher frequency noise can significantly degrade the quality of the reconstructed image, introducing unwanted artifacts and reducing the overall clarity. To address this, a series of masks were strategically placed within the optical path to ensure the beam remains band-limited, filtering out undesirable spatial frequencies and maintaining control over essential frequencies for a cleaner amplitude profile. (Blinder et al. (2022))

Initially, a 7mm aperture mask was applied at the beginning of the benchtop generator to ensure that the beam size matched the 7mm phase screen of the SLM. This step was essential to maintain the correct beam profile and prevent any discrepancies in the size of the light field interacting with the SLM. Following this, a second mask was placed at the focal plane after the reflection off the first SLM. The primary purpose of this mask was to eliminate the extra frequency noise surrounding the amplitude before the beam was superimposed with the second phase. This higher frequency noise can originate from imperfections in the SLM and other optical components, and if not properly filtered, it can lead to significant distortions in the final image.

Figure 3.6 illustrates the impact of these masking steps. The left image shows the irradiance or intensity without any spatial frequency masking, highlighting the presence of substantial noise and artifacts. The image on the right demonstrates a significant reduction in spatial noise around the amplitude after the initial mask was introduced before the first SLM pass. This reduction in noise is crucial for achieving a higher fidelity in the reconstructed image.

To further enhance the quality of the amplitude profile, another mask was implemented before the second SLM phase pass. This additional mask aimed to reduce the extra frequency noise from the first phase prediction model. By filtering out these high-frequency components, the system could produce a more accurate and stable amplitude profile, which is essential for the subsequent phase manipulation.

After initial data collection, it became apparent that a third aperture mask might be

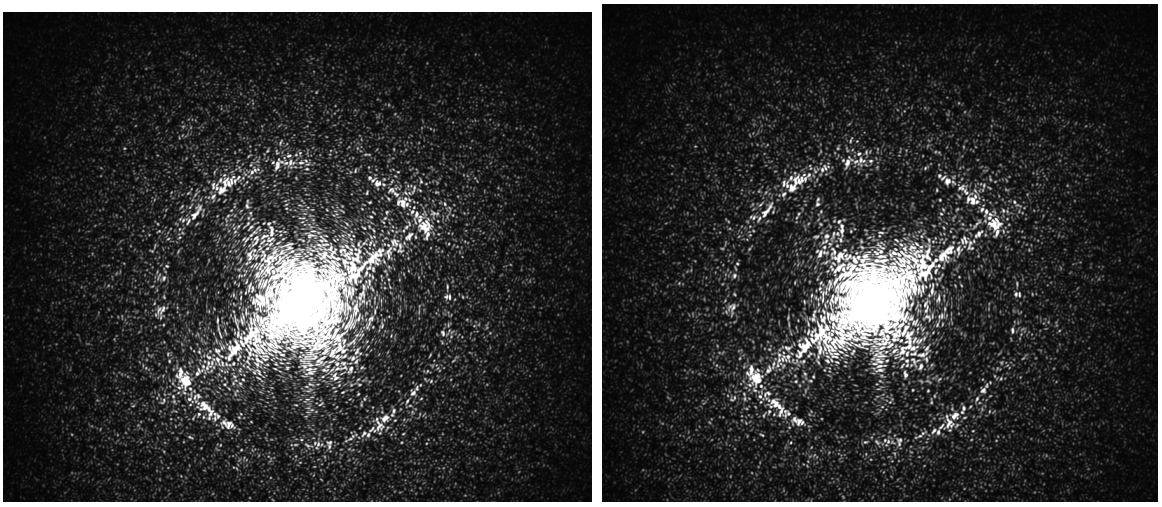

Figure 3.6 *Left: Saturated amplitude, for better visualization, without spatial frequency masking. Right: Amplitude after applying the first aperture mask.*

necessary to address any remaining higher frequency noise implemented in the phase after the second SLM pass. This iterative process of masking and alignment is crucial for achieving high-fidelity image reconstruction in the optical system. The combination of these masks significantly improved the quality of the amplitude profile, reducing noise and enhancing the clarity of the final image. This systematic approach to eliminating higher frequency noise underscores the importance of careful optical design and precise alignment in achieving optimal performance in complex wavefront manipulation systems.

The addition of these masks was pivotal in enhancing the overall quality of the optical system. By strategically eliminating higher frequency noise at various stages of the optical path, the system could produce clearer and more accurate images, thereby demonstrating the critical role of spatial frequency filtering in advanced optical applications.

3.7 Polarization

Polarization is a critical factor in optical systems involving Spatial Light Modulators (SLMs), as it can significantly affect the performance and accuracy of the wavefront modulation. The SLMs used in this setup operate effectively only with specific polarization states of light. Therefore, it is essential to control the polarization state of the laser beam before it interacts with the SLMs and after it has been modulated.

To achieve this control, a half-wave plate was implemented at the beginning of the bench-top setup and another one was placed after the first SLM pass. The half-wave plate functions by rotating the plane of polarization of the incoming light. When light passes through a half-wave plate, its polarization direction is rotated by twice the angle between the light's initial polarization direction and the optical axis of the half-wave plate. This allows precise adjustment of the light's polarization state.

In the initial stage of the benchtop setup, the laser beam's polarization state needed to be adjusted to match the required input polarization state of the first SLM. The half-wave plate was rotated to ensure that the light entering the SLM was polarized correctly. This step was crucial because improper polarization can lead to inefficiencies in modulation and can introduce errors in the phase and amplitude control.

After the light beam was modulated by the first SLM, its polarization state was altered due to the reflection off of the SLM. To correct this and prepare the beam for subsequent modulation by the second SLM, a second half-wave plate was placed after the first SLM. This half-wave plate was adjusted to rotate the polarization back to the desired state for the

second SLM.

The implementation of the half-wave plates provided several benefits including improved modulation efficiency by ensuring that the light entering each SLM was correctly polarized and the modulation efficiency of the SLMs was maximized. This helped in achieving the desired phase and amplitude modulation with higher accuracy. It also reduced errors. Misalignment in polarization can introduce phase errors and reduce the contrast of the modulated light. The half-wave plates helped in minimizing these errors, leading to more precise control of the wavefront. They also provide flexibility in adjustments. The use of half-wave plates allowed for easy and precise adjustments of the polarization state without the need to alter the optical components or the laser source. This flexibility was essential for fine-tuning the system and optimizing its performance. Lastly, different SLMs may have specific polarization requirements for optimal operation. The half-wave plates ensured that these requirements were met, making the system compatible with various types of SLMs used in the experimental setup.

3.8 Scaling and Sampling

There is a scaling or sampling issue due to pixel size difference between the SLM BMPs, the original image of Hubble used, and the camera used. Because of this, the generated phase screens and amplitude needed to be scaled in order to size to the correct 7mm pupil on the SLMs. This caused a sampling issue, resulting in poor resolution. Figure 3.7 shows an example of the phases before and after scaling to show the resolution change. This

diminish in resolution adds to the error in the final dual phase image, which is already of poor resolution and difficult to see.

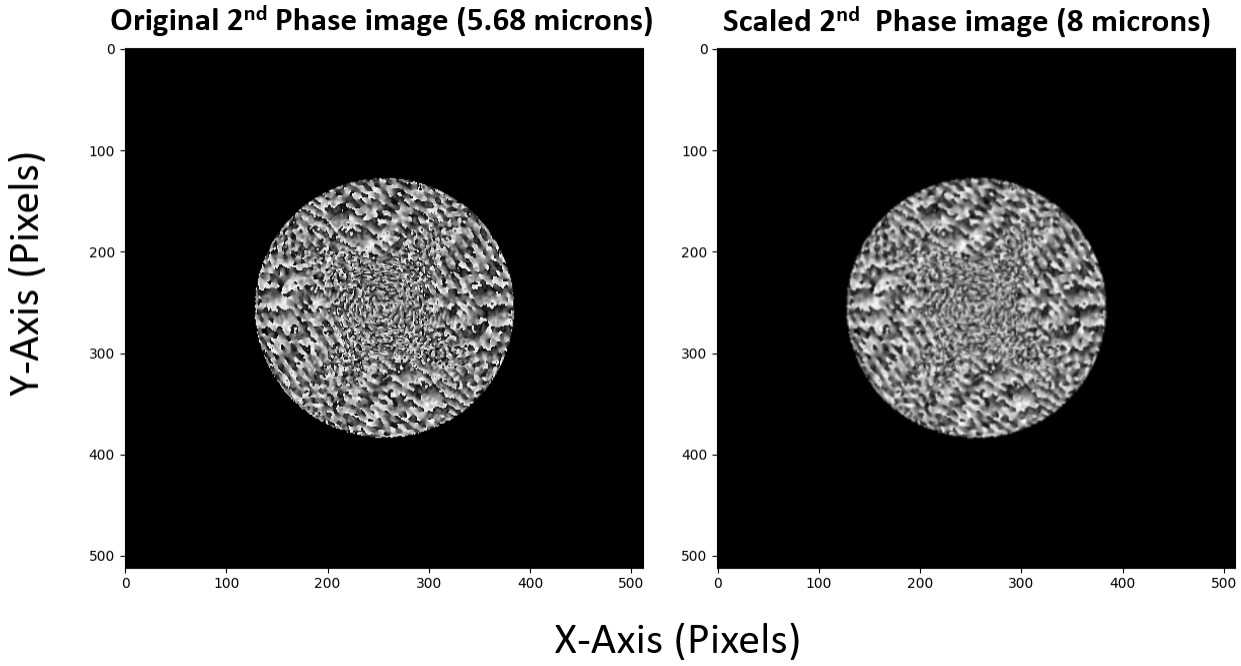

Figure 3.7 *Right: Phase image after scaling, showing worse resolution. This scaling issue gets implemented into the final image, causing significant concerns.*

In the future, to avoid losing any resolution, the images used need to be the same size as the required SLM size. Ensuring that the image dimensions match the SLM specifications will preserve the resolution and enhance the clarity of the final output.

3.9 New Setup

In an attempt to remove spherical aberrations and alignment issues, I implemented a second Spatial Light Modulator (SLM) into the optical system. The inclusion of an additional SLM was aimed at mitigating the effects of lenses and simplifying the optical path, thereby

enhancing the precision and stability of the setup. Two lenses were removed from the original design to streamline the setup for easier alignment and debugging.

Aligning an optical setup that involves multiple lenses and a single SLM is a highly intricate process, especially when implementing a blaze grating. The precision required to position each lens accurately and ensure the SLM is perfectly aligned with the optical axis is immense. Any slight misalignment can lead to significant errors in the diffraction pattern, reducing the effectiveness of the blaze grating. To minimize these alignment challenges and associated errors, the setup was reconfigured to use two SLMs and a single lens. This modification simplified the alignment process and reduced the potential for misalignment, as the optical path became less complex.

The new setup design incorporated an addition SLM. The second SLM was introduced to provide additional phase control, allowing for more precise wavefront manipulation. This dual-SLM configuration enabled the system to correct for aberrations and enhance the fidelity of the optical simulations. By removing two lenses from the optical path, the setup was simplified. This reduction in optical components decreased the chances of misalignment and minimized the sources of potential aberrations introduced by the lenses. The simplified optical path made it easier to achieve and maintain precise alignment. This was crucial for ensuring that the phases generated by the SLMs were accurately superimposed and that the final image quality was not compromised. With fewer components to align, the precision of the setup was significantly improved. The use of two SLMs allowed for independent phase adjustments, making it easier to fine-tune the system and correct for any misalignments or

aberrationss.

The construction of the improved setup began in the lab, incorporating these changes and aiming to enhance the overall system performance. The new configuration was assembled, starting with the precise placement of the two SLMs. Each SLM was carefully aligned with the optical axis, ensuring that the laser beam passed through the center of the SLMs without any deviation. Calibration of the SLMs was performed to ensure that the phase modulation was accurately controlled. This involved adjusting the input polarization and verifying the output phase patterns. The alignment of the entire optical path was verified using a optical mounted pin holes as well as mirrors. A camera was used after each lens to verify focus position. This step was crucial to ensure that all components were correctly positioned and that the beam path was free from obstructions or deviations. Fine-tuning of the alignment was carried out by making small adjustments to the positions of the SLMs and the remaining lens that were all on x,y stages as well as kinematic magnetic mounts for easy removal. The goal was to achieve perfect overlap of the phases generated by the two SLMs.

Initial tests were conducted to evaluate the performance of the new setup. The output phase and amplitude patterns were analyzed to identify any remaining alignment issues or aberrations. Debugging involved iterative adjustments and re-calibrations to refine the setup. Any identified issues were addressed by making precise modifications to the optical path and alignment. However, due to time constraints involving construction in the lab as well as available tools, the enhanced setup and improved phases were not fully tested. Despite this, preliminary observations indicated several potential benefits of the new setup.

The dual-SLM configuration showed promise in enhancing the image quality by providing more accurate phase modulation. The ability to independently control two phases allowed for better correction of wavefront distortions. The removal of two lenses and the simplified optical path contributed to a significant reduction in spherical aberrations and other distortions. This improvement was expected to enhance the overall clarity and fidelity of the final images. The simplified setup was easier to align and maintain. The reduced number of optical components made it less prone to misalignment, leading to more stable and consistent performance.

Future implementation of this new setup, which includes the use of two SLMs and a single lens, along with higher-resolution phase images, is expected to yield a final image that closely resembles the model by adding a flat image tot he second SLM for phase screen corrections, as well as a third polarizer after the second SLM. The anticipated improvement in image quality will validate the modifications and demonstrate the effectiveness of the refined optical configuration.

The new setup provides a robust framework for future experiments. By addressing the issues related to spherical aberrations and alignment, the dual-SLM configuration holds the potential to achieve higher accuracy and performance in wavefront manipulation. Further testing and optimization will be necessary to fully realize the benefits of this setup and to refine the phase generation process.

3.10 Second Phase Technique

Implementing a second phase for amplitude manipulation in the optical system was a critical step aimed at improving the resolution and overall quality of the generated images. Hsieh et al. (2007) The need for a second phase arises from the inherent limitations of using a single phase to control both the amplitude and phase of the light field. A single phase often results in incomplete amplitude modulation, increased noise, and phase-amplitude coupling, making it difficult to achieve precise manipulation of the light field. To address these issues, a dual-phase system was implemented, using two SLMs to independently control the amplitude and phase, thereby enhancing the modulation capabilities and improving the image quality.

The methodology for implementing the second phase involved several key steps. Initially, the design was simulated using Zemax to understand the behavior of the dual-phase system, predicting the phase patterns and identifying potential challenges. Figure 3.8 shows the output from a one-phase only model, highlighting the limitations in amplitude modulation and the resulting image quality.

The experimental setup was reconfigured to include two SLMs, as detailed in the New Setup section, involving precise alignment of the SLMs and calibration of their phase modulation capabilities. The dual-SLM configuration was tested with various input patterns to evaluate its performance. Figure 3.9 shows the results from the two-phase model and the corresponding benchtop output.

Despite these improvements to the optical benchtop, the dual-phase system presented challenges in terms of alignment and calibration. Precise alignment of the two SLMs was

critical to achieving the desired results, and any misalignment could introduce errors. The current setup relied on manual adjustments, which limited the precision of the alignment. Future implementations may benefit from motorized mounts to achieve more accurate and repeatable positioning.

The experiments also highlighted the need for further optimization, as the system was sensitive to environmental factors such as vibrations from shared table movements, which affected the stability of the alignment as well as the level of the laser beam which changed daily. Future work will focus on addressing the remaining challenges and further optimizing the setup. Incorporating motorized mounts and automated alignment systems will enhance the precision and repeatability of the setup, reducing the time and effort required for manual adjustments and improving the overall stability. Developing more sophisticated algorithms for phase generation will further improve the accuracy and efficiency of the dual-phase system, leveraging machine learning techniques to optimize the phase patterns based on real-time feedback.

Using SLM like devices with higher resolution and better performance characteristics will enhance the modulation capabilities, allowing for finer control over the light field and further improving the image quality. SLM pixel limitations contributed to the resolution limits highlighted in Burger et al. (2008). Extensive testing with a variety of input patterns and conditions will help in identifying and addressing any remaining issues, ensuring the robustness and reliability of the dual-phase system for practical applications. In conclusion, the second phase technique represents a significant advancement in the field of optical wavefront

manipulation. By providing independent control over amplitude and phase, the dual-phase system enhances the resolution and quality of generated images, paving the way for more accurate and reliable optical simulations.

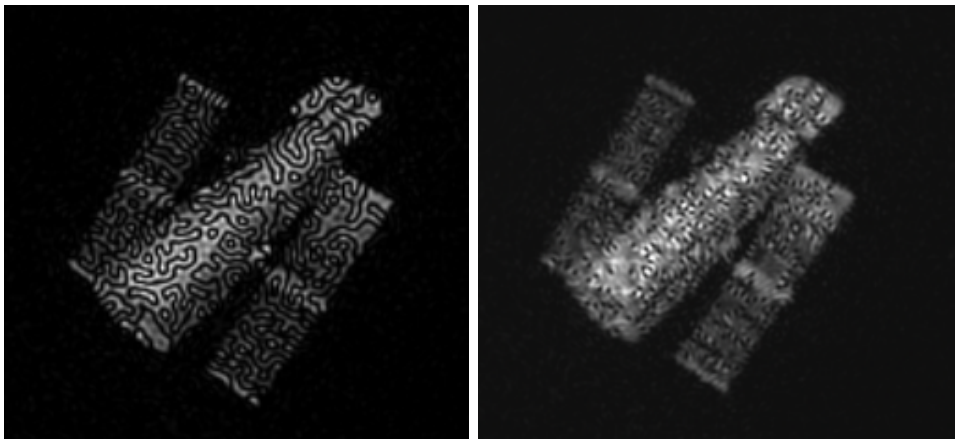

Figure 3.8 *Left: Image from a one-phase only model. Right: Benchtop one-phase output from the lab.*

The comparison between the one-phase and two-phase modeled images illustrates the significant improvements achieved with the dual-phase simulated or modeled approach. Figure 3.8 shows the limitations of the one-phase system, with the simulated and benchtop outputs exhibiting noticeable noise and reduced resolution.

To further investigate the potential of the two-phase method, An image of the amplitude from the benchtop setup was taken using the CCD camera at the focal plane and superimposed with the generated second phase using computational techniques. The Fourier transform was then applied to this composite image and confirmed that the Hubble image was indeed produced. However, the resulting image was very noisy and did not account for the additional noise and diffraction effects that would be introduced during the second SLM pass in the physical setup. in figure 3.10, the left image presents the superimposed squared

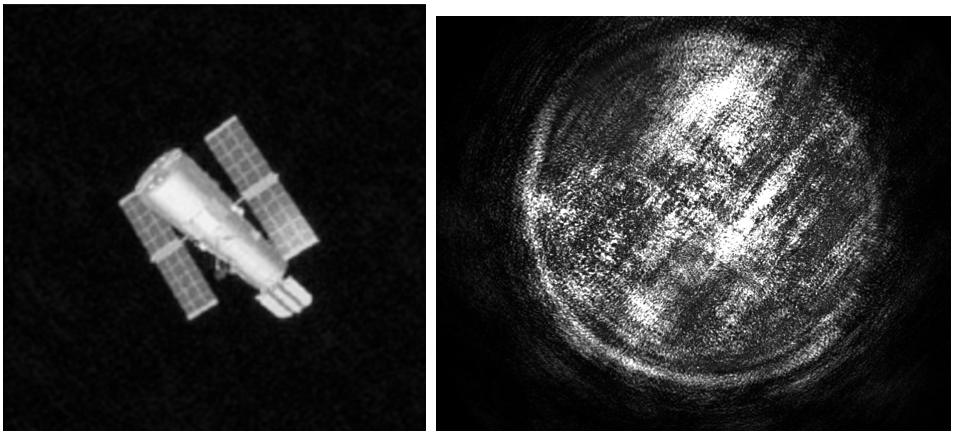

Figure 3.9 *Left: Object or image generated from the two-phase model. Right: Initial object generated from the benchtop using the two-phase wavefront manipulation tool.*

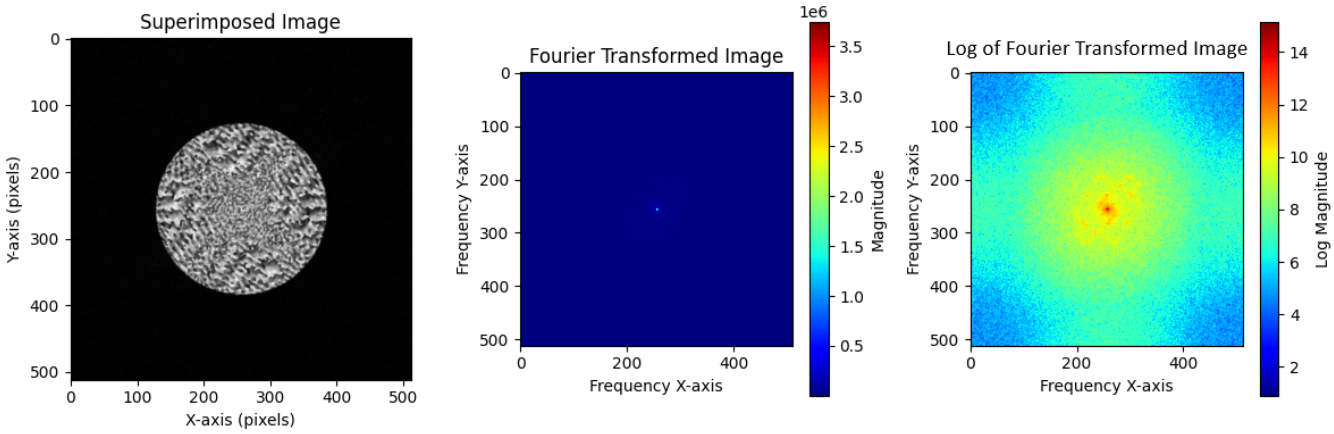

Figure 3.10 *Left: Amplitude image in the form of intensity generated and captured after the Fourier transform of the first phase off of the first SLM pass. Middle: The superimposed image of the squared intensity image and the second phase after a Fourier transform. Right: The superimposed image in log form for better visualization.*

intensity and second phase image. The middle plot shows an outline of the faint hubble image located in the very center. To better visualize the outcome, the right image displays the superimposed Fourier transformed image in log form with a color map to enhance the outline of the Hubble image.

This experiment highlights the challenges of the current setup and suggests that it is

nearly impossible to achieve a high-quality two-phase image with the existing configuration. The above-mentioned improvements, such as motorized mounts for precise alignment and higher resolution components, are necessary to successfully and efficiently produce a resolved better image each time.

Enhancing Research in Optical Physics and Astronomy

The object generator allows researchers to simulate complex light fields and optical phenomena under controlled laboratory conditions. By precisely modulating the amplitude and phase of light wave fields, the system can replicate the appearance of celestial bodies or artificial satellites as viewed through Earth's turbulent atmosphere. Zhang et al. (2013) This capability is invaluable for testing hypotheses, validating theoretical models, and conducting experiments that would otherwise require impractical, expensive, or impossible observational telescopes.

4.1 ARES System

The ARES (Adaptive Real-time Engine Simulator) system represents an advancement in optical simulation technology, providing an emulation of the effects of atmospheric turbulence on astronomical observations, as outlined in Abbott et al. (2022) ARES integrates spatial light modulators (SLMs) with adaptive deformable mirrors to create a dynamic simulation environment that reflects the variable nature of atmospheric interference on starlight. This environment enables precise modeling of atmospheric turbulence, essential for studying its impact on celestial imaging and refining adaptive optics (AO) systems crucial for correcting atmospheric distortion.

The object generator module will enhance ARES's capabilities by allowing it to simulate a diverse array of targets, from artificial satellites to natural celestial bodies. This tool will

modulate the amplitude and phase of light, thereby creating realistic simulations of various objects. Jesacher et al. (2008) Once implemented, the object generator will enable comprehensive simulation scenarios that include both object generation and atmospheric effect emulation. This will increase the system's flexibility and applicability across educational and professional scenarios, facilitating a deeper understanding of complex atmospheric phenomena and adaptive optics operations, and preparing future astronomers and engineers for real-world astronomical observations.

4.2 Advancements in Space Surveillance and Situational Awareness

For space agencies and defense organizations, the ability to accurately simulate various objects in space is critical for developing and testing space surveillance systems. Zhang et al. (2013) These systems rely on the detection, tracking, and characterization of objects in orbit to maintain situational awareness and ensure the safety of satellites and crewed missions. The object generator's capacity to mimic the optical signatures of satellites, debris, and other space objects under varying conditions aids in improving the algorithms and sensors used for space surveillance, enhancing our ability to monitor and respond to potential threats or collisions in orbit.

4.3 Improvements in Adaptive Optics Systems

Adaptive optics (AO) systems are designed to correct distortions in light caused by atmospheric turbulence, enabling telescopes to achieve clearer images of astronomical objects. Roddier (1999) The object generator's ability to simulate these distortions and the corre-

sponding optical targets provides a powerful tool for testing and refining AO systems. By evaluating how well an AO system can correct simulated distortions and accurately reproduce the target image, researchers and engineers can identify improvements, leading to better performance of telescopes and imaging systems on the ground and in space.

4.4 Facilitating the Development of Optical Communication

Optical communication systems, including those used for satellite communication, rely on the precise transmission and reception of light signals. The object generator can simulate the effects of atmospheric turbulence on these signals, allowing for the testing and optimization of communication systems to ensure reliable data transfer. This is particularly important for the development of global communication networks and deep space communication, where signal integrity is critical. Hsieh et al. (2007); NASA (2023)

4.5 Educational and Training Applications

The object generator can also serve as an educational tool, providing students and trainees with hands-on experience in observing and analyzing simulated optical phenomena. This practical exposure can enhance learning and understanding of complex concepts in optics, astrophysics, and atmospheric science, preparing the next generation of scientists and engineers with valuable skills and knowledge.

Conclusion

The research presented in this thesis focused on constructing and refining a benchtop wavefront manipulation system, inspired by the work of Jesacher et al. (2008). This work involved replicating their two-phase, two-pass modulation system using Spatial Light Modulators (SLMs) to achieve precise control over both spatial amplitude and phase distributions. The ability to manipulate these parameters can benefit simulating complex optical scenarios and improving the quality of astronomical observations.

Through this research, significant advancements were made in understanding and implementing the dual-phase system. The introduction of additional components, such as masks to remove unwanted spatial frequencies and half wave plates to control the polarization state of the laser beam, played a critical role in enhancing the overall quality of the system. These modifications addressed some of the practical challenges faced in the implementation of a simulated or modeled holography two phase technique.

The modeling and simulation work using Zemax provided valuable insights into the behavior of the optical system, highlighting potential issues with alignment and phase modulation. This approach allowed for the optimization of the setup. Despite these advancements, achieving precise alignment in a dual-phase system remains a significant challenge. The experiments conducted demonstrated the potential of the dual-phase system to enhance image resolution and clarity. However, the current setup faced limitations in achieving high-quality two-phase images, primarily due to the complexity of alignment and the noise introduced

during the second SLM pass. Future improvements, such as the implementation of motorized mounts for precise alignment and the use of higher-resolution components, are necessary to overcome these challenges and realize the full potential of the dual-phase system.

The work presented in this thesis lays the groundwork for further advancements in wavefront manipulation and PSF engineering. The developed benchtop wavefront manipulation system represents a significant step forward in the field, offering a scalable, hardware-based tool for a wide range of applications, from astronomical observations to space surveillance. By continuing to refine and optimize this system, future research can build upon these findings to achieve even greater accuracy and performance in optical simulations and real-world applications.

REFERENCES

Abbott, C., et al. 2022, in 2022 Advanced Maui Optical and Space Surveillance Technologies Conference

Arines, J., & García, A. 2020, Optical Engineering, 59, 041206

Blinder, D., Birnbaum, T., Ito, T., & Shimobaba, T. 2022, Light: Advanced Manufacturing, 3, 572

Burger, L., Litvin, I. A., & Forbes, A. 2008, South African Journal of Science, 104, 129

Hope, D. 2019, in Advanced Maui Optical and Space Surveillance Technologies Conference

Hsieh, M.-L., Chen, M.-L., & Cheng, C.-J. 2007, Optical Engineering, 46, 070501

Improso, W. D. G. D., Tapang, G. A., & Saloma, C. A. 2019, Suppression of Zeroth-Order Diffraction in Phase-Only Spatial Light Modulator, ed. P. Ribeiro, D. L. Andrews, & M. Raposo (Cham: Springer International Publishing), 1–30

Jeffries, S. 2024, Personal communication, verbal discussion

Jesacher, A., et al. 2008, Optics Express, 16, 2597

Miura, N. 2003, Optics Letters, 28, 2312

NASA. 2023, Optical Communications Overview, accessed: 2024-07-28

O'Neill, E. 1956, IRE Transactions on Information Theory, 2, 56

Roddier, F. 1999, Adaptive optics in astronomy (Cambridge University Press)

Suchkov, N., Fernández, E. J., Martínez-Fuentes, J. L., Moreno, I., & Artal, P. 2019, Optics Express, 27, 12399

Tyson, R. K. 2014, Principles and applications of Fourier optics (IOP Publishing, Bristol, UK)

Zhang, W., Jiang, Z., Zhang, H., & Luo, J. 2013, in 2013 Seventh International Conference on Image and Graphics, IEEE, 721–726